# Long-Range Oxidative Damage in DNA/RNA Duplexes†

Duncan T. Odom and Jacqueline K. Barton*

*Division of Chemistry and Chemical Engineering, California Institute of Technology, Pasadena, California 91125*

*Received February 12, 2001; Revised Manuscript Received May 31, 2001*

ABSTRACT: Oxidative damage as a result of DNA-mediated long-range charge transport occurs readily and at high yield in duplex DNA, and it is of interest whether similar damage can occur in duplex oligonucleotides that include both ribo- and deoxyribonucleotides. Assemblies containing RNA and mixed RNA·DNA strands were constructed containing tethered ethidium as a photooxidant. In photooxidation experiments, long-range oxidative damage to the ribose-containing strand of the oligonucleotide duplexes was examined. Hole injection by photoexcited ethidium followed by radical migration to oxidatively susceptible guanines afforded significant damage on ribose-containing strands at long range (∼35 Å). This damage does not differ substantially in yield and location from that found in B-DNA duplexes. No oxidative damage was found upon photooxidation of DNA/RNA duplexes containing tethered metallointercalator, despite the ability of the rhodium complex to promote oxidative damage at a distance in DNA duplexes. This result is attributed to the poor coupling of the rhodium complex into the A-like RNA/DNA duplex. The ability for long-range charge transport to occur in double-stranded nucleic acids of different comformations is considered in light of modeling studies that show interstrand base−base overlap between the opposing, complementary strands that make up RNA/DNA hybrid duplexes. Thus, the possibility of long-range radical migration to effect oxidative damage or signaling may be considered also in the context of transcriptional events.

Recently, the ability of DNA to both mediate and participate in charge transport has been the subject of considerable research (*1*−*12*). Oxidative damage to DNA is suspected to play significant roles in processes as disparate as aging and cancer, and understanding the molecular basis of genetic degradation has become an important research goal (*13*−*15*). In addition, recent nanotechnological research has highlighted on the possible uses of DNA duplexes as possible one-dimensional quantum wires and templates for directed material deposition (*16*), and larger nucleotide assemblies as building blocks for nanoscale structures and signaling devices (*17*−*20*). Dissecting possible roles that the $\pi$-stack can play in long-range charge transport, and the precise parameters for this reaction are of fundamental interest.

The heteroaromatic $\pi$-stack of duplex DNA plays a critical role in facilitating long-range charge transport to effect oxidative damage to DNA at a distance from the location of an introduced electronic hole (*1*−*8*). Typically, a photooxidant is appended covalently to one site of a duplex, and electronic holes are injected into the base stack by these oxidants at a known location. In our laboratories, we have focused on appending metallointercalators to stack near the terminus of the DNA duplex (*4*). As a result of long-range charge transport, the injected radical then localizes onto the 5′-guanine of 5′-GG-3′ doublets, the most oxidatively sensitive sites (*21*). Subsequent trapping of the radical with $H_2O$ or $O_2$ leads to formation of an irreversible lesion that is easily visualized by denaturing gel electrophoresis after treatment with base (*22*). Many different covalently attached photooxidants have been used to cause this type of long-range damage, including metallointercalators (*23*), ethidium derivatives (*24*), anthraquinone derivatives (*25*, *26*) and flavins (*27*). All of these photooxidants can easily access the electronic structure of the base stack by intercalating into or stacking onto the end of the DNA helix, whereas photooxidants that cannot electronically access the base stack in this manner have not been observed to damage the 5′-guanine of a guanine doublet from a distance (*28*). Studies have shown that modifying the structure of the base stack, for instance by the introduction of bulges (*30*), mismatches (*31*, *32*), or protein binding (*33*, *34*), can affect charge transport. Although considerable discussion exists as to the exact mechanism of radical migration through the base stack (*2*, *5*, *35*−*40*), electron and hole hopping between bases and domains is almost certainly involved (*11*, *25*, *41*).

Other experiments have applied fluorescence quenching to investigate electron transport in DNA (*42*, *43*). DNA base analogues that have donor and acceptor properties, but that still form hydrogen bonds to complementary bases, can be introduced into DNA at known locations (*42*). Because these bases retain their usual base-pairing properties, their duplexes are in standard B-form, and the distance and orientation between donor and acceptor are precisely known. By varying the location and orientation of these two species, fluorescence quenching as a function of distance was probed. When both donor and acceptor are on the same strand, the rate of electron transfer is significantly more rapid than when they are on opposing strands; intrastrand charge transport in B-DNA is more facile than interstrand charge transport.

† Supported by NIH Grant GM49216.

* To whom correspondence should be addressed. E-mail: jkbarton@caltech.edu.

10.1021/bi0102961 CCC: $20.00 
Published on Web 07/06/2001

Long-range radical migration has also been investigated in non-B-form DNA. It was found that migrating charges can access single-strand overhangs from a duplex region that has had a radical injected into it (*44*). Interestingly, the preference for 5′-guanine damage in a guanine doublet was eliminated; instead, guanines were evenly damaged regardless of surrounding base identity. Similar experiments have shown that triple-stranded DNA, both in short oligonucleotides (*45*) and in plasmid fragments (*46*), can promote charge transport over significant distances. Our continuing interest in long-range charge transport in various nucleic acids led us to investigate the RNA/DNA hybrid duplex as a possible medium for radical migration.

In solution, heteroduplexes of RNA and DNA assume conformations between the A-form of RNA duplexes and the B-form of DNA duplexes, and are central to genetic biochemistry (*47*−*52*). Reverse transcriptases, most prominently HIV reverse transcriptase, produce RNA/DNA hybrids when replicating viral genomes. RNA/DNA hybrids are also found during transcription of a DNA template into a mRNA transcript. Furthermore, in DNA replication, lagging strand synthesis is initiated by synthesis of a short RNA oligonucleotide by primase, from which are formed Okazaki fragments.

Some research investigating long-range charge transport in RNA/DNA hybrids and part ribose, part deoxyribose containing chimeric nucleic acid (CNA)/DNA hybrids has been carried out (*53*). These studies focused on oxidative damage that occurs on DNA strands in a DNA/RNA or DNA/CNA hybrid. Long-range oxidative damage of guanines was observed at 35 °C, but not at 20 °C, and no preference was observed for oxidative lesions to localize on the 5′-G of a 5′-GG-3′ doublet. The low levels of strand cleavage were attributed to the hydrophobic nature of the A-like structure of the RNA/DNA hybrid duplex. No inspection of the damage that may occur on the RNA strand or segment was conducted.

Here, we demonstrate that long-range transport occurs efficiently through the RNA strand of an RNA/DNA duplex to the 5′-guanine of 5′-GG-3′ doublets. We utilized base sequences used previously to explore the role of the DNA/DNA $\pi$-stack as a bridge for remote oxidation (*24*). As in previous studies (*53*), our results indicate that RNA/DNA hybrids can act as a bridge for electron transfer. However, in contrast to previous results (*53*), we find that radical migration occurs in similar amounts in RNA/DNA hybrids to that found in purely DNA duplexes at ambient temperature, and that the resultant oxidative damage in both cases is overwhelmingly localized to the 5′-guanine of a 5′-gg-3′ doublet.

## MATERIALS AND METHODS

*Materials*. All chemical reagents and starting materials were purchased from commercial sources and used as received. Et′[1] and its methyl ester were synthesized as previously described (*43*).

Oligodeoxynucleotides were synthesized on an ABI 392 RNA/DNA synthesizer with trityl protecting groups and purified by C18 reverse-phase HPLC. These oligonucleotides were then detritylated and HPLC-purified a second time. Ethidium-modified (*43*) and rhodium-modified (*54*) oligodeoxynucleotides were prepared according to published procedures, and stored in dried aliquots at −70 °C until needed.

*RNA Synthesis*. RNA oligonucleotides and chimeric RNA·DNA hybrids were prepared on an ABI 392 RNA/DNA synthesizer entirely with fresh reagents, and deprotected using standard techniques. These deprotected, desilanized sequences were purified using a preparative-scale, nondenaturing, 10% polyacrylamide gel. The desired sequence was visualized by rapid UV shadowing, cut from the gel, crushed, and eluted at 4 °C overnight into 10 mL of RNase-free 50 mM Tris·HCl, pH 7.5, with 1 mM EDTA (TE). This solution was loaded onto a 12 $cm^3$ Sep-Pak cartridge using standard procedures and rinsed extensively with water and the oligonucleotide eluted with 10 mL of 50% aqueous acetonitrile. The purified oligonucleotide was stored in aliquots at −70 °C as a dry solid, and redissolved as needed.

*RNA and DNA Techniques and Photoirradiation Experiments*. The oligonucleotides used were 5′-end-labeled using [$\gamma$-$^{32}$P]ATP and polynucleotide kinase. The reaction mixture was desalted, treated for 30 min with either 1 M piperidine at 90 °C (DNA) or 1 M aniline acetate at 60 °C (RNA and RNA·DNA hybrids), and purified on a 20% nondenaturing acrylamide gel. The desired band was cut from the gel, and soaked in 3 × 1 mL of TE buffer, and isolated by use of NENsorb 20 oligonucleotide columns (Dupont) using standard procedures. Samples used in irradiations were annealed on a thermocycler by heating to 90 °C for 5 min, followed by linear cooling to 4 °C over 90 min. Noncovalent intercalators, when used, were added after duplex annealings were complete.

Irradiations were performed at 22 °C on 10 $\mu$L samples in pre-siliconized 1.5 mL Eppendorf tubes using a 1000 W Hg/Xe arc lamp equipped with a monochromator. Samples were prepared in 17 mM sodium salt phosphate buffer at pH 7.0, 50 mM NaCl, and contained 10 $\mu$M duplex strands. In experiments where intercalator was bound noncovalently to the duplex, the concentration of Et′OMe was also 10 $\mu$M. After irradiation, the samples were dried by vacuum concentration. These samples were then either directly diluted into formamide gel loading buffer or heated for 30 min in a total volume of 100 $\mu$L in the presence of 1 M piperidine (90 °C), or 1 M aniline acetate (60 °C) for all-DNA and RNA-containing samples, respectively, to reveal oxidative damage. Drying in vacuo was followed by dissolution into denaturing, formamide-based gel loading buffer. Sequencing gels were 20% denaturing polyacrylamide containing 8 M urea, and were analyzed by phosphorimagery.

*Calculation of Base*−*Base Overlaps*. Using an $O_2$ SGI workstation and InsightII software with Biopolymer Module, idealized stick-drawn B-form DNA dinucleotides were assembled. These nucleotides were centered down the dyad axis, and frame pictures were taken. After exporting to a Macintosh G3, these pictures were opened by Adobe PhotoShop, and the overlap between the stacked bases was shaded. Hardcopy prints of these photographs were made, and the stick structures were cut out and weighed to determine the partitioning of overlap between neighboring bases. The same procedure was followed for the DNA/RNA hybrid duplexes, using the A-form DNA/RNA tool.

[1] Abbreviations: phi, phenanthrenequinone diimine; bpy′, 4-butyric acid, 4′-methylbipyridine; DMB, 4,4′-dimethylbipyridine; Et′, *N*-8-glycylethidium.

## RESULTS

*Experimental Design.* To investigate the ability of RNA/DNA hybrids to mediate long-range hole transfer, ethidium was used as a photooxidant in many of our experiments. Ethidium can intercalate into both A- and B-form DNA, as seen by luminescence enhancement when this intercalator is bound to either duplex RNA or B-form DNA (*55*, *56*). Because of the non-B-form structure of the duplexes used in this study, the ability to intercalate into A-form, B-form, and forms intermediate to these two was an essential requirement for the photooxidant. Previous studies in our laboratory have shown that ethidium, when photoexcited, can cause radical migration through DNA, and subsequent guanine oxidation at a distance (*24*). Here, as previously, covalently bound ethidium showed significant damage at the guanine located at its intercalation site after irradiation at 313 nm, consistent with the direct formation of a covalent lesion at the site of intercalation. Conjugates of Rh(phi)$_2$bpy′$^{3+}$ with the same sequence were used to compare the effect photooxidant stacking has on the ability of an intercalator to introduce radicals into the base stack; phi complexes of rhodium are not expected to intercalate effectively into A-form nucleic acids (*57*, *58*).

To facilitate comparison with previous work, base sequences identical to those found in earlier reports (*24*) were utilized in these studies (Figure 1). These sequences contained guanine doublets proximal and distal to the tethered photooxidant. The sugar identity of the strand complementary to the one bearing the tethered photooxidants was varied to focus on the role(s) that conformation plays in enabling long-range oxidation. The strands were synthesized as phosphoramidites, and purified by nondenaturing gel electrophoresis. The strand integrity was verified by radiolabeling with polynucleotide kinase, and inspecting the band pattern on a denaturing 20% polyacrylamide sequencing gel.

*Guanine Oxidation in an RNA/DNA Hybrid Duplex by Photoexcited Ethidium.* DNA-GG duplexes with tethered ethidium as a photooxidant showed, as expected, oxidation at the 5′-guanine of the 5′-GG-3′ sites upon photoirradiation. Direct damage to the guanine located at the ethidium intercalation site is also evident when photoirradiated at 313 nm for an hour, indicating the site of association (Figure 2). Hence, oxidation at the 5′-GG-3 sites results from a long-range transport event. By annealing the same ethidium-bearing strand to a complementary RNA strand, RNA−GG is assembled (Figure 1). Subsequent photoirradiation followed by aniline treatment showed that, as with exclusively DNA assemblies, sites of greatest damage are the 5′-guanines in 5′-GG-3′ doublets. Moreover, the ethidium intercalation site also shows damage that corresponds closely with that seen in DNA/DNA hybrids irradiated under the same conditions, due to the direct reaction of excited-state ethidium with the adjacent guanine. As with DNA-GG, here too oxidative damage at the guanine doublets is the result of radical migration from a distance.

Notably, when either DNA-GG or RNA-GG is photoirradiated in the presence of noncovalently bound, equimolar ethidium, the proximal guanine doublet is not damaged, though both the distal site guanine and the intercalation site guanine still show oxidation (Figure 2). The reason for this lack of reaction at this site is not clear. In addition, the RNA constructs show consistently higher backgrounds and degrade more rapidly than do exclusively DNA assemblies.

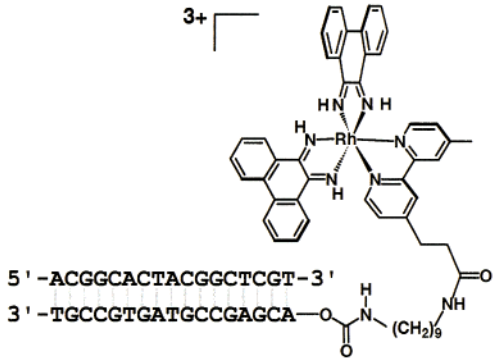


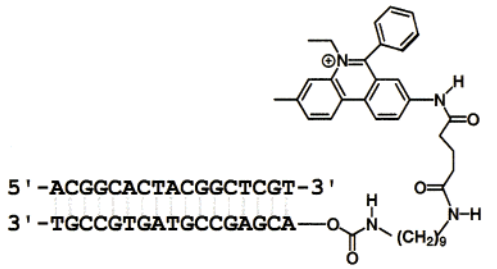


*5'-ACGGCACTACGGCTCGT-3'
3'-TGCCGTGATGCCGAGCA-5'(-Int)

**DNA-GG**

*5'-acggcacuacggcucgu-3'
3'-TGCCGTGATGCCGAGCA-5'(-Int)

**RNA-GG**

*5'-AcggcACTAcggcTCGT-3'
3'-TGCCGTGATGCCGAGCA-5'(-Et')

**CNA-GG**

*5'-ACAACACTACAACTCGT-3'
3'-TGTTGTGATGTTGAGCA-5'(-Et')

**DNA-AA**

*5'-AcaacACTAcaacTCGT-3'
3'-TGTTGTGATGTTGAGCA-5'(-Et')

**CNA-AA**

FIGURE 1: Nucleic acid duplexes used to investigate long-range radical migration. The assemblies are named based on the sugar composition of the second strand, followed by the base composition of the sites of oxidation, and can have ethidium, Rh(phi)$_2$bpy′$^{3+}$, or no photooxidant covalently tethered to the 5′ end of one of the strands. Thus, DNA-GG represents an assembly where the strand complementary to the intercalator is entirely DNA with guanine doublets. RNA-GG has a complementary strand entirely of ribose sugars and guanine doublets; CNA-GG has a chimeric mixture of RNA and DNA with guanine doublets; DNA-AA contains a DNA strand with adenines in place of guanines; and CNA-AA contains a chimeric strand with adenine doublets. −Int in the figure represents the attachment site of a generic intercalator.

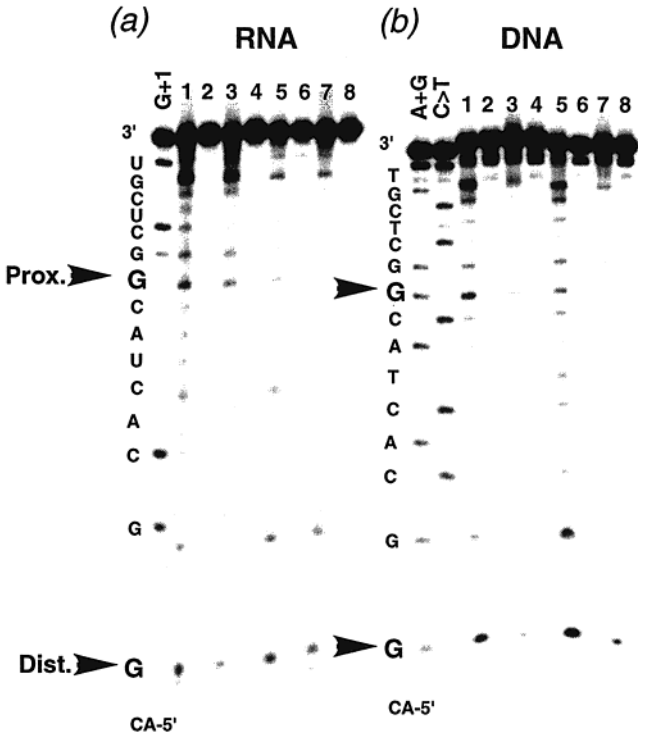


FIGURE 2: Long-range guanine damage in RNA-GG duplexes (a) and DNA-GG duplexes (b) with covalently attached Et′. Shown is the phosphorimagery of a representative 20% denaturing gel. Lanes are as follows: G+1, RNase T1 digestion; A+G, C>T, Maxam−Gilbert sequencing reactions; lane 1 is 313 nm irradiation with hot base treatment (10% piperidine at 90 °C with DNA, 1 M aniline acetate at 60 °C for RNA); lane 2 is nonirradiated duplex with base treatment; lane 3 is 313 nm irradiated duplex without base treatment; lane 4 is nonirradiated duplex without base treatment; lanes 5−8 are identical to lanes 1−4, but with noncovalent Et′ used with unmodified duplexes, instead of covalently attached intercalator. All irradiations were performed for 1 h, and the following concentrations were used: 10 $\mu$M duplex, 17 mM sodium phosphate, pH 7.0, buffer, 10 $\mu$M ethidium methyl ester in experiments with noncovalent intercalator. The sequence of the oligonucleotides is shown to the left of each panel, with the reactive guanines in slightly larger font, boldface, and indicated by arrows.

Quantitation of the oxidative damage for the different constructs is shown in Table 1. The amount of direct strand scission caused at the binding site guanine by photoexcitation of the intercalated ethidium is assumed to correlate with the amount of ethidium intercalation. The damage that is seen at the guanine located at the ethidium binding site is largely independent of base treatment, consistent with previous results that indicate that this intercalator is able to cause direct strand scission at guanines when photoexcited at an appropriate wavelength (*24*).

In the analysis presented here, the direct damage at this guanine is determined by subtraction of the respective dark control from the photoirradiated but not base-treated sample; this procedure varies slightly from that performed in quantitating long-range oxidation, where the amount of damage is determined by subtracting the base-treated and irradiated samples from those that were irradiated but not treated with base. The resulting value reflects the binding of ethidium. Averaging this experiment over three trials reveals that the actual damage intensity at this location is from 2 to 3 times that found at the distal sites. To assess absolute yields of damage, ratios are presented for distal and proximal guanines normalized to the direct damage as calculated above at the intercalation site. Also shown are the ratios of distal to proximal damage, which, based on the above reasoning, is a measure of the efficiency of charge transport through a sequence.

Table 1: Partitioning between Oxidatively Damaged Sites in RNA/DNA and DNA/DNA Duplexes[a]

| second strand | RNA | DNA | CNA |
|---|---|---|---|
| covalent Et′ distal/prox | 0.6 (0.2) | 1.1 (0.1) | 0.9 (0.2) |
| covalent Et′ prox/direct | 0.5 (0.2) | 0.3 (0.05) | N/A |
| covalent Et′ dist/direct | 0.3 (0.1) | 0.3 (0.05) | N/A |

[a] These ratios were obtained by comparing the direct damage at the intercalation site guanine by photoexcited ethidium that is not dependent on base treatment, and the base-dependent 5′-guanines of 5′-GG-3′ doublets proximal and distal to the ethidium-bearing end of the duplex. Each number is the average of three trials. Experimental conditions are described in the caption to Figure 2, and under Materials and Methods of this paper.

*Guanine Oxidation in an RNA/DNA Hybrid Duplex by Photoexcited Rhodium Complex*. Effective coupling between the intercalator injecting the radical and the base stack which mediates the charge transport is required for efficient charge migration. To demonstrate this, the ethidium intercalator was replaced with a metallointercalator previously shown to have a strong preference for B-form DNA over the A-form. Here, a derivative of $[Rh(DMB)phi_2]^{3+}$ was tethered to a DNA oligonucleotide and subsequently annealed with RNA to form the substrate duplex RNA-GG (Figure 1), and photoirradiation of these assemblies was performed at both 313 and 365 nm. Damage can be seen at the binding site upon irradiation at 313 and 365 nm when the complementary strand is either RNA or DNA, as is evident with RNA-GG in Figure 3. However, little oxidative damage is evident at 5′-GG-3′ doublets. This observation is consistent with the close, albeit nonintercalated, binding of the rhodium complex. Instead, limited depurination is evident throughout the duplex, and the first, proximal guanine doublet shows slight oxidative damage. In contrast, efficient long-range charge transport in rhodium complex-coupled DNA-GG occurs at both oxidatively sensitive sites (not shown). Therefore, we conclude that because the rhodium complex is ineffective at intercalating into the RNA/DNA hybrid, it is ineffective at promoting oxidative damage at a distance through the RNA/DNA hybrid duplex.

*Guanine Oxidation in an CNA/DNA Hybrid Duplex by Photoexcited Ethidium*. Having shown that RNA/DNA hybrids can efficiently support radical migration when the photooxidant is well-coupled into the base stack, we investigated also the effect of junctions between regions of ribose and deoxyribose sugars (CNA-GG) on long-range charge transport. The oxidatively sensitive 5′-CGGC-3′ cassettes were replaced in the parent DNA sequence with the RNA cassette 5′-cggc-3′, thus creating a strand with discrete regions of ribose and deoxyribose sugars. After annealing the strands to form the duplex CNA-GG that contains a covalently attached ethidium, photoirradiations were performed, as previously. After photooxidation, the guanine doublets appear to show some damage, but it is modest (Figure 4). Considerable nonspecific damage also occurs in these constructs. Notably, the single guanine proximal to the intercalated ethidium shows lower than expected damage from direct reaction with the photooxidant.

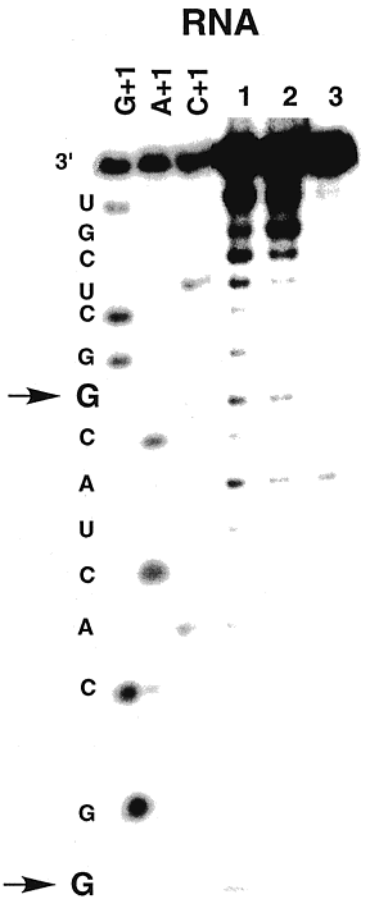


FIGURE 3: Intercalation site and long-range guanine oxidative damage in RNA-GG duplexes when $[Rh(phi)_2bpy']^{3+}$ is covalently appended. Sequencing lanes are as in Figure 2. Other lanes are as follows: lane 1, photoirradiation for 1 h at 365 nm with aniline treatment; lane 2, photoirradiation for 10 min at 313 nm, no base treatment; lane 3, nonirradiated samples with aniline treatment. In all irradiations, the following concentrations were used: 10 $\mu$M duplex, 17 mM sodium phosphate, pH 7.0, buffer.

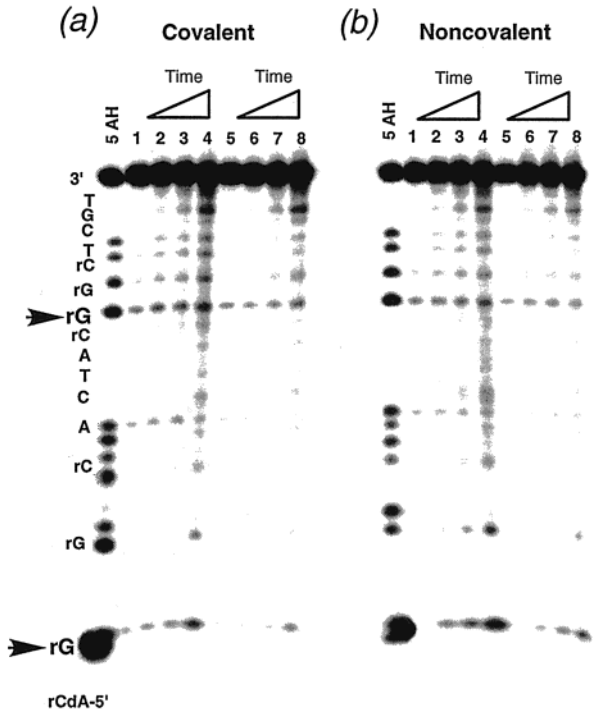


FIGURE 4: Long-range oxidative damage at 5′-gg-3′ cassettes in CNA-GG. Sample concentrations are as in Figure 2. The sequence, shown to the left of panel (a), was determined by alkaline hydrolysis (AH) of the RNA-containing regions. AH lanes were exposed to 50 mM $Na_2CO_3$, pH 11, for 5 min. Sequencing hydrolysis cleavage occurs one base pair from the oxidative cleavage site. Lanes 1−4 of each panel are 15, 30, 60, and 120 min irradiations followed by aniline acetate treatment of the samples; lanes 5−8 are the same irradiation times without aniline treatment.

It is important to note that we have assigned the location of the damage observed to the guanine sites by comparison with the sequencing reactions. Sequencing reactions were performed by alkaline hydrolysis of the RNA-containing regions. Basic hydrolysis marks a site that is one base upstream of the site of strand scission by base-liberated oxidative damage. Damage to the heterocyclic base and subsequent cleavage cause loss of the sugar−phosphate attached to it. In contrast, intramolecular hydrolysis at the 3′-hydroxyl attached to the same base leaves the sugar−phosphate intact. Thus, direct hydrolysis of the 3′-hydroxyl affords a fragment that is one base longer than oxidative reactions.

In contrast to the relatively modest damage that occurs at the intercalation site, the sites damaged most severely comigrate with the expected location for guanine oxidation. Much of this damage can be attributed to hydrolysis, a particular issue for oligonucleotides containing RNA−DNA junctions. This assumption is further supported by the dependence of the damage on aniline treatment (Figure 4). All analyses of oxidative damage, therefore, subtracted the nonirradiated samples as controls. In addition, experiments where the CNA-GG duplex was incubated with noncovalent ethidium, and photooxidation reactions performed, showed that aniline-dependent damage occurred at the same sites, further supporting the contention that these are the sites of oxidative susceptibility.

*Oxidation in a Duplex Lacking Guanine Doublets by Photoexcited Ethidium*. To verify that the damage seen here is specific to guanine, the 5′-CGGC-3′ cassettes were replaced with 5′-CAAC-3′ cassettes to afford DNA-AA and CNA-AA target strands. As can be seen in Figure 5, neither construct, when assembled with covalently tethered ethidium and photoirradiated, showed any significant damage except at the lone remaining guanine at the intercalation site. This site corresponds to that of lowest oxidation potential in this sequence; the result confirms that the damage seen earlier is indeed guanine-specific.

*Analysis of Base−Base Overlaps in RNA/DNA and DNA/DNA Duplexes*. Using the InsightII program to generate the structures of idealized dinucleotides, we calculated the base−base overlaps that occur in different canonical duplexes (Table 2). These dinucleotides only represent static snapshots of idealized configurations for nucleic acids in solution. Furthermore, our calculations of these overlaps give preference to the occlusion of the ring systems, as the stick bonds used to trace the shortest line between atom centers were arbitrarily chosen to define the base surface area. In heteroaromatic bases of nucleic acids, this assumption in effect biases the overlap calculations toward the ability of these ring systems to stack with overlapping $\pi$-clouds. Even in our modeling, all of the dinucleotides are in van der Waals contact. Clearly, this analysis neglects the considerable $\pi$-overlap that occurs with exocyclic carbonyls and amines. Ideally, these effects could be investigated with much more

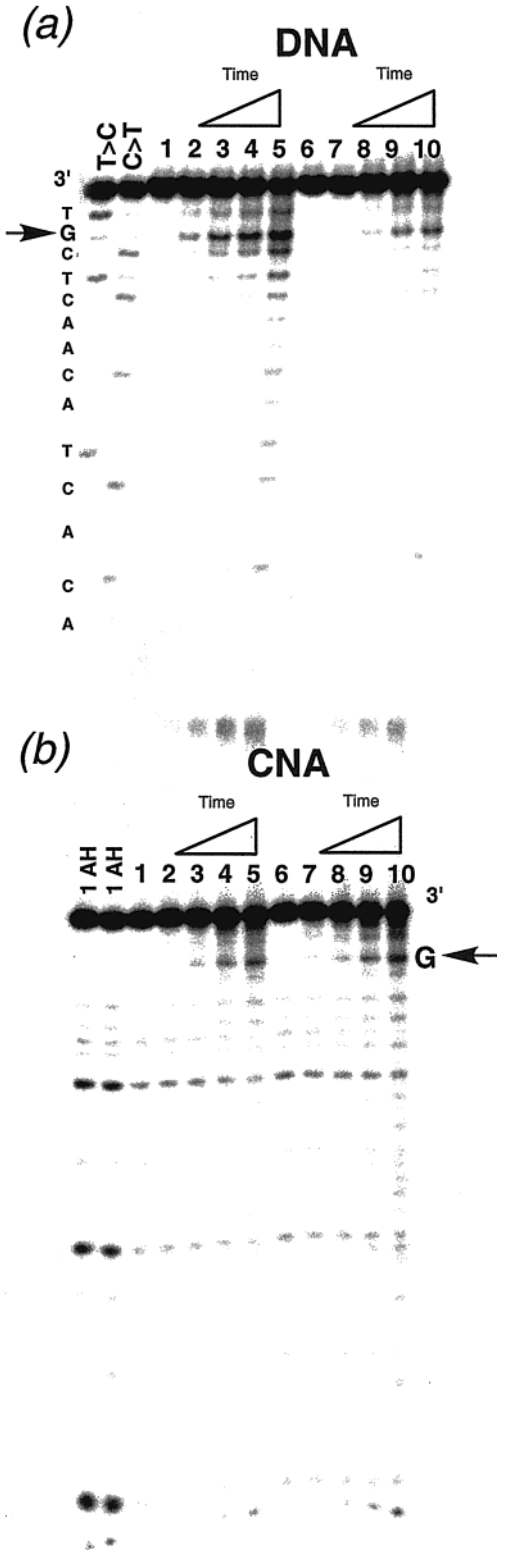


FIGURE 5: Oxidative damage found in the absence of guanine doublets in ethidium-tethered DNA-AA (a) and the equivalent result in CNA-AA (b). No damage is apparent in either case, except at the guanine located at the intercalation site.

computationally intense and exacting modeling, but the ideal dinucleotides that we use give a general picture of the inter- and intrastrand stacking that occurs.

As is evident in Table 2, purine−purine (R−R) steps are extremely well-stacked, with typical intrastrand overlaps of their aromatic rings greater than one-fourth of the surface area. Purine−pyrimidine (R−Y) steps have intrastrand overlaps comparable to those for R−R steps on the purine base, but with even greater coverage (exceeding 50% of the surface area in some cases) for the pyrimidine base. Pyrimidine−pyrimidine (Y−Y) junctions in all cases have minimal to no overlap. Most interestingly, however, pyrimidine−purine (Y−R) steps, which in DNA/DNA duplexes have no overlap, show appreciable *intrastrand* overlap between the purines on opposite strands when in an idealized A-form RNA/DNA duplex. Exemplifying these data, two base steps, 5′-CG-3′ and 5′-GG-3′, are shown in Figure 6 in both A- and B-conformations.

## DISCUSSION

The ability of photooxidants to damage guanine at a distance by long-range charge transport in ribose-containing nucleic acids is governed by multiple factors. First, radical injection must occur efficiently. Second, this generated radical must propagate through the intervening base steps to an oxidatively sensitive site. Third, the site oxidized must be thermodynamically and kinetically reactive on the time scale of the radical lifetime, and a lesion must be formed that can be visualized by chemical or biochemical means. Figure 7 summarizes the results obtained; the experiments conducted in this study provide considerable information about the relationship of nucleic acid conformation to these factors.

*Efficient Radical Injection Is a Prerequisite for Long-Range Charge Transport*. Clearly, without efficient radical injection into the base stack, charge transport is not possible. The differing ability of ethidium and $[Rh(phi)_2bpy']^{3+}$ to induce guanine oxidation at a distance when conjugated to duplexes of the same sequence demonstrates this dependence. Previous studies investigated the guanine oxidation that occurs in DNA duplexes conjugated to ethidium, and the results here for DNA-GG coupled to ethidium are, as expected, in line with previous reports, including the damage yield and partition ratios between sites (Table 1). In RNA-GG with covalently tethered ethidium, long-range charge transport occurs to the same locations as in DNA-GG and with roughly the same yield (Figure 2 and Table 1), unambiguously demonstrating efficient radical injection. Because of the facile intercalation and high-affinity binding of ethidium in both A-form and B-form nucleic acids, upon photoirradiation, this intercalator can efficiently inject a radical into the base stack, regardless of the stacking orientation and sugar conformation(s).

In contrast, the irradiation of similar duplexes, but with $[Rh(phi)_2bpy']^{3+}$ covalently tethered to the end of the duplex in place of ethidium, affords considerably different results. In normal B-form DNA, irradiation at 313 nm of phi complexes of rhodium promotes cleavage of DNA backbone sugars at intercalative binding sites via direct hydrogen abstraction from the sugar ring (*59*). Using this convenient photochemistry to mark the sites of binding, it is evident that the metal complex is bound near the end of the duplex. Photoirradiation of $[Rh(phi)_2bpy']^{3+}$-tethered DNA duplexes at 365 nm leads to injection of a high-energy radical into the base stack (*8*). Migration of this charge, and subsequent localization onto an oxidatively sensitive site, causes irreversible lesions that can be revealed with hot base treatment. In DNA-GG, photoirradiating this duplex at 365

Table 2: Base Surface Overlap in Idealized Dinucleotides

| DNA/RNA sequence[a] | % 5′-base surface area overlap (intrastrand)[b] | % 3′-base surface area overlap (intrastrand)[b] | % DNA 3′-base area surface overlap (interstrand)[b] | % RNA 3′-base area surface overlap (interstrand)[b] | DNA/DNA sequence[a] | % 5′-base area surface overlap[b] | % 3′-base area surface overlap[b] |
|---|---|---|---|---|---|---|---|
| 5′-AA | 26 | 26 | – | – | 5′-AA | 27 | 27 |
| 5′-AG | 26 | 26 | – | – | 5′-AG | 29 | 28 |
| 5′-GA | 28 | 29 | – | – | 5′-GA | 28 | 28 |
| 5′-GG | 28 | 28 | – | – | 5′-GG | 33 | 33 |
| 5′-AT | 42 | 67 | – | – | 5′-AT | 20 | 33 |
| 5′-AC | 37 | 59 | – | – | 5′-AC | 25 | 37 |
| 5′-GT | 42 | 29 | – | – | 5′-GT | 21 | 52 |
| 5′-GC | 43 | 72 | – | – | 5′-GC | 22 | 36 |
| 5′-TT | 0 | 0 | – | – | 5′-TT | 5 | 5 |
| 5′-TC | 0 | 0 | – | – | 5′-TC | 4 | 4 |
| 5′-CT | 0 | 0 | – | – | 5′-CT | 4 | 4 |
| 5′-CC | 0 | 0 | – | – | 5′-CC | 3 | 3 |
| 5′-CG | – | – | 19 | 19 | 5′-CG | 0 | 0 |
| 5′-CA | – | – | 18 | 18 | 5′-CA | 0 | 0 |
| 5′-TG | – | – | 18 | 18 | 5′-TG | 0 | 0 |
| 5′-UA | – | – | 26 | 26 | 5′-TA | 0 | 0 |

[a] Dinucleotides of the sequences listed were generated as idealized duplexes in Insight II using the Biopolymer Module. Since both strands are fitted to ideal parameters, the overlaps found in the dinucleotides of both strands of the RNA/DNA hybrid duplexes are identical. [b] Base area overlaps were obtained as follows. Photographs of the dinucleotides were obtained by centering the view directly down the dinucleotide axis in InsightII. The pictures were exported into Photoshop 4.0.1, classified as overlap or nonoverlap base area, and then cut out and weighed. These weights were assumed to correspond directly to area, and used to calculate the percentage overlap. Errors in measurement are estimated to be 5%.

nm affords roughly equal partitioning of oxidative damage between the proximal and distal sites. In contrast, RNA-GG, when tethered to $[Rh(phi)_2bpy']^{3+}$, shows almost no oxidative damage at the 5′-gg-3′ sites that were strongly damaged at a distance by photoexcited ethidium (Figure 3). The low yield of guanine oxidation at a distance in RNA-GG, despite appreciable damage at the site of metal complex binding, is probably due to groove binding of the covalently tethered $[Rh(phi)_2bpy']^{3+}$. This nonintercalative reaction is driven by tethering; electrostatics also may play some role. The metal complex is not tightly stacked between the bases in the case of RNA-GG because it cannot fit into the narrow major groove associated with A-like conformation of the nucleic acid, in contrast to the wide major groove of B-form duplex DNA. No photocleavage within A-form duplex regions was seen in previous studies with phi complexes of rhodium when noncovalently bound to tRNA (*58*).

*Propagation of Charge through the Base Stack and Radical Trapping*. Estimates of the charge transport efficiency, once a radical is successfully introduced into the base stack, can be made by comparing the distal versus proximal ratios of guanine oxidation. This ratio is determined by the ability of a charge to migrate through the base stack between two sites, and directly reflects the capacity for a nucleic acid to act as a bridge for radical migration. In addition, the ratio of the direct damage caused by ethidium at its site of intercalation to the damage seen at oxidatively sensitive sites located a distance from the binding site of the photooxidant can be calculated and used to determine absolute yields. Notably, this estimate of absolute yield assumes that radical trapping is comparable between RNA and DNA strands. Our data suggest that this assumption is correct, based on the high levels of long-range guanine oxidation that occur with ethidium-coupled RNA-GG, and the similarities between the RNA and DNA distal/proximal ratios and overall yield of oxidative damage (Table 1). Although this supposition appears to be valid for RNA-GG and DNA-GG for the reasons outlined, CNA-GG duplexes appear to be less specifically damaged at the ethidium intercalation site. This lower level of damage may represent a conformation at the binding site that is less favorable toward direct reaction.

Distal/proximal ratios were calculated for each of the ethidium-tethered constructs, DNA-GG, RNA-GG, and CNA-GG. As expected, the ethidium-tethered DNA-GG has a partition ratio of 1, within the uncertainty of the experiment. Notably, ethidium-tethered RNA-GG, which contains a second strand of purely ribonucleic acid, shows slightly more damage at the proximal guanine doublet than does its ethidium-tethered DNA-GG counterpart. Taking into account the uncertainty in this series of experiments, RNA-GG has a somewhat lower distal/proximal ratio compared to DNA-GG. These data suggest that RNA is a viable conduit for charge transport but perhaps poorer than the B-form DNA duplex. Certainly the closeness of the ratios suggests that the stacking interactions in the core of the duplex are more important to radical migration than the identity of the sugar and global conformation of the assembly. Not unexpectedly, the distal to proximal ratio for CNA-GG is between that of RNA-GG and DNA-GG. Therefore, it seems likely that the base stack of CNA-GG may have more B-form character than that of RNA-GG.

The absolute yield of charge migration can be estimated by normalizing the guanine oxidation that occurs remotely at the distal site to the direct damage induced by photoexcited ethidium at its binding site. Taking the ratio of the distal doublet to the direct damage as a benchmark measure, covalently bound ethidium is seen in both RNA-GG and DNA-GG to be a very efficient photooxidant. Typically, guanine doublets located distal to the site of intercalation show approximately 30% of the guanine oxidation that occurs by direct contact with photoexcited ethidium. Thus, a significant percentage of the radicals introduced into the base stack by photoexcited ethidium, when either DNA or RNA is the complementary strand, migrate to a remote site and are irreversibly trapped. The absolute yield of long-range

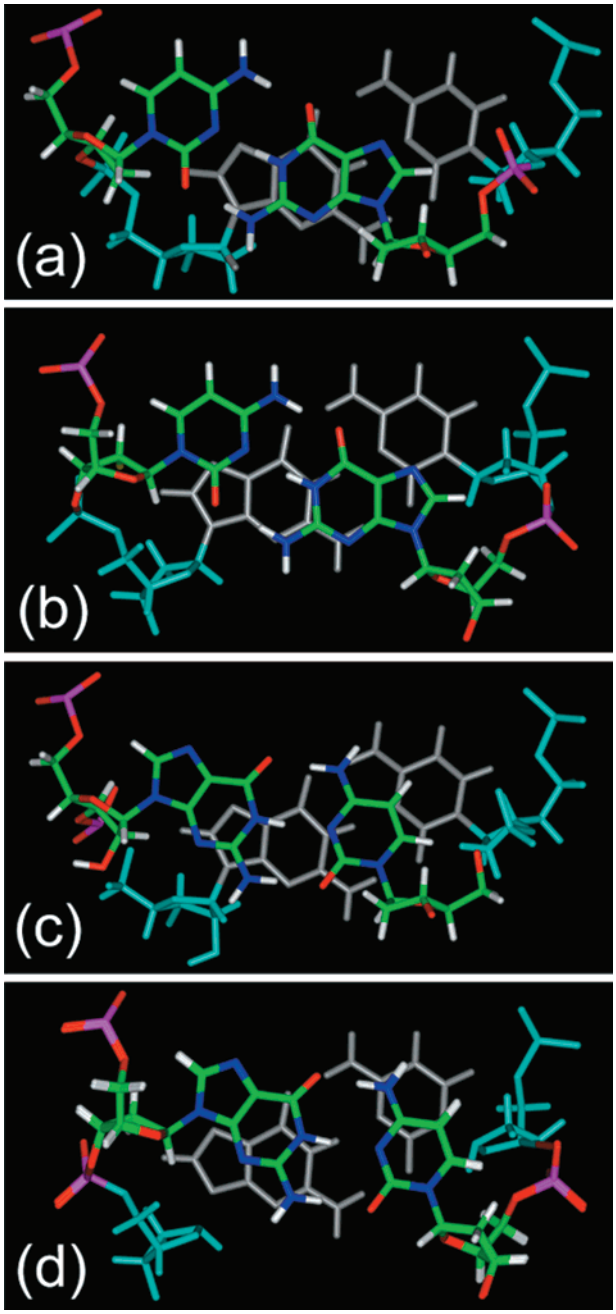


FIGURE 6: Selected ideal dinucleotide base overlaps in A-form and B-form nucleic acids. The 5′ base and sugar are colored by atom type, and the 3′ 'underlying' base is colored light blue for the sugar and gray for the base. Views are directly down the helical axis. (a) A-form 5′-CG-3′, (b) B-form 5′-CG-3′, (c) A-form 5′-GG-3′, (d) B-form 5′-GG-3′. Comparison of panels (a) and (b) reveals that the interstrand overlap in A-form 5′-CG-3′ (discussed further in the text) is caused by overlap of the six-membered ring of the purine bases. Contacts exist between the purine rings in the B-form (panel b) but are limited to the edges of the six-membered rings. Panels (c) and (d) clearly show that the overlap present in 5′-GG-3′ is comparable in magnitude between these two different forms, but differs in alignment.

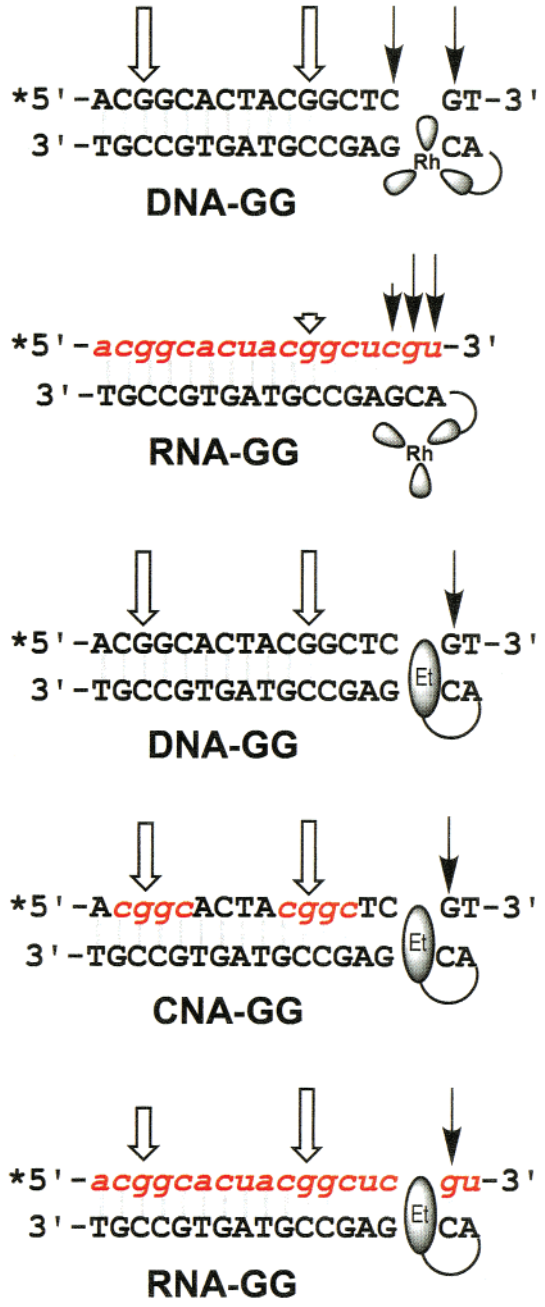


FIGURE 7: Schematic illustration of the oxidative and direct damage seen in each duplex investigated here. The name assigned in Figure 1 is shown to the right of each duplex, and oxidative damage levels shown by arrows are approximate (quantitative values are found in Table 1). Hollow arrows indicate the oxidative damage revealed by hot base treatment, while the black arrows represent direct strand scission location for rhodium-appended nucleotides and direct base reaction locations with ethidium. The first two duplexes are rhodium complex-tethered[ the latter three are ethidium-tethered.

guanine oxidation, however, is negligible when the rhodium intercalator is used as a photooxidant in RNA-GG. This diminution is most likely the result, not of an inability of the nucleic acid to transport charge, but of poor electronic coupling between the metallointercalator and the RNA-GG base stack.

*Effect of Ribose·Deoxyribose Junctions on Electron Transport*. Ethidium-tethered CNA-GG shows damage at a distance after photoirradiation, but little damage at the intercalation site. The direct trapping of the radical at the binding site in CNA-GG may follow a different mechanism than in RNA-GG or DNA-GG, or possibly the same mechanism has an appreciably lower yield. This low yield for the direct reaction precludes discussion of absolute yields in CNA-GG constructs, as without a reliable value for the direct damage, it is impossible to estimate the amount of interca-

lative binding by ethidium, and to relate this value to damage at a distance.

Previous research that introduced a single ribose sugar in an otherwise entirely DNA duplex can induce an entire duplex to assume an A-like conformation in the solid state (*60*, *61*), but solution studies using NMR suggest somewhat more complicated conformations with deoxyribose sugars assuming a more B-like structure and ribose regions tending to A-form (*47*). Hence, CNA-GG may have a structural junction between regions of ribose versus deoxyribose sugars, but the overall stacking of the duplex bases is expected to be continuous. Clearly, the distal to proximal ratio demonstrates efficient charge migration to remote sites of oxidative sensitivity in this chimeric duplex.

*Comparison with Previous Studies*. Our results provide an interesting comparison and contrast to the damage on DNA strands of RNA/DNA hybirds reported previously (*53*). Previous research showed that oxidative damage partitioned roughly equally between sites distal and proximal to a covalently linked anthraquinone when oligonucleotides were between A-form and B-form. However, the absolute yield was decreased greatly, and the 5′-guanines of 5′-GG-3′ doublets were no longer the most sensitive oxidatively. The low yield was attributed to trapping effects, and further experiments increasing the temperature and, thus, B-form characteristics of the hybrid duplexes seemed to increase the overall yield of oxidative damage. Presumably, the trapping of the generated guanine radical was greatly improved with increasing B-form character of the constructs. Indeed, in the most A-like structures previously investigated, no long-range oxidative damage at all was seen in homosaccharide RNA/DNA duplexes on the DNA strands. Importantly, however, no measure of anthraquinone binding was provided for normalizing the reactions.

In contrast to this decrease in yield, our duplexes show comparable yields of oxidative damage between DNA duplexes and RNA/DNA hybrids, as estimated based on ratios to the direct damage at the intercalation site. The partitioning of radical damage between oxidative sites in our duplexes, like those seen previously, seems to be largely independent of the sugar composition of the oligonucleotide. However, long-range charge transport and its trapping at susceptible guanines *on the RNA strand* of an RNA/DNA hybrid duplex seem to be almost identical in magnitude as in B-form DNA/DNA duplexes of the same base sequence. Similar experiments in previous studies that focused on the damage on the DNA strand of an RNA/DNA hybrid found considerably reduced yields at oxidatively sensitive guanine sites (*53*).

It is also clear from our results that coupling of the photooxidant into the duplex is a critical parameter governing the efficiency of long-range charge transport. Just as we observed a poor yield with $[Rh(phi)_2bpy']^{3+}$-coupled duplexes, perhaps this inefficient coupling can account in part for the results with anthraquinones (*53*). Since little structural data are available, it is certainly possible that the anthraquinones are not stacked closely or perhaps evenly on the top of the A-form RNA/DNA duplex, and, thus, are poorly electronically coupled to the guanine doublets. Direct comparison of the two systems by radiolabeling of the intercalator-bearing strand and performing photoirradiations of the subsequent assembly would be desirable. In the case of our complexes, however, decomposition of the functionalized strand in base makes such experiments difficult.

Furthermore, the RNA/DNA hybrids here display oxidative damage patterns on the RNA strand that are equivalent to those found when purely DNA/DNA hybrids are used. Other researchers have suggested that RNA/DNA hybrids, at least on the DNA strand bearing a photooxidant, lose the hallmark damage at the 5′-guanine in 5′-GG-3′ doublets (*53*). Clearly, our results show that the 5′-guanines of 5′-GG-3′ sites retain their preferred oxidative susceptibility when on an RNA strand.

*Radical Migration and Base Overlap*. To explore theoretically whether long-range coupling through the stacked aromatic heterocycles of A-form nucleotides was feasible, molecular modeling was also used to estimate the overlap of idealized A-form RNA/DNA hybrid dinucleotides and B-form DNA duplex dinucleotides. Although we found that the base−base overlaps on the whole were quite comparable between the two conformations, there were notable differences, as illustrated in Figure 6. Most importantly, B-form DNA shows little base−base overlap between the two separate strands that make up the duplex. In contrast, in A-form nucleotides, significant *interstrand* base overlap is found in a number of cases, notably between the adjacent guanines in 5′-CG-3′ steps (Figure 6a).

One implication of this interstrand overlap not directly explored here is the possibility that long-range charge transfer, which is sensitive to stacking and also is strand-specific in B-form DNA, may equilibrate more rapidly between the two duplex strands when they are in conformations that approach the A-form. The potentially greater electronic coupling between the two strands could significantly change the pathway by which radicals propagate through the base stack. Previous results have shown that in duplex B-form DNA a difference of 3 orders of magnitude in rate was evident in comparing interstrand base−base electron transfer to intrastrand electron transfer (*42*). The results here suggest that this difference may not hold in A-like conformations. Indeed, it is possible that ribose-containing nucleic acids show a slightly steeper distance dependence due to the diffusion of the migrating radical into the second strand; any damage that occurred on the second strand to trap the radical would be undetectable by our methodology.

An equally important issue raised here is the relative susceptibility of guanine doublets toward oxidation in duplexes in and between A- and B-conformations. Again, in computer modeling of guanine doublets, the overlap seen between neighboring intrastrand guanines was quite significant in both A-form and B-form. Note that the B-form guanine doublet overlap obtained through this modeling differs somewhat in each of the two studies for which overlaps have been shown previously (*62*, *63*). The alignment for the two conformations (A-form and B-form) in our modeling study also differs (Figure 6c,d). Because of this, it is possible that the oxidation potentials are not equivalent in these two cases; however, it is clear that guanine doublets, experimentally, are found to be the most sensitive sites for oxidative damage on the RNA strand of RNA/DNA hybrids, as well as in B-form, duplex DNA. This suggests that even if the exact trapping mechanism is different between these two cases, the rate of trapping appears to be quite comparable

between a B-form DNA strand and a more A-form RNA strand. Otherwise, the yields at the guanine doublets between different nucleic acid conformations would vary greatly.

Our finding that mixed nucleotides can support radical migration efficiently is consistent with the effective stacking found in idealized A-form constructs. Hence, consistent with previous results, it appears that the most critical parameter that determines electronic coupling is the ability for the bases' aromatic surfaces to stack regularly, though the overall conformation of the sugar backbone and the three-dimensional location and orientation of the base strands can vary quite widely.

*Conclusions*. In summary, RNA/DNA hybrids can act as conduits for long-range oxidative damage, comparable to DNA/DNA counterparts of an identical sequence. Hence, it is possible that oxidative damage can occur at a distance when a radical is introduced on the RNA strand generated by DNA-to-RNA transcription, polymerase priming, and Okazaki extensions. The results described here underscore the inherent tendency for well-stacked nucleic acids to act as bridges for charge migration, regardless of the identity of the sugars. Remarkably, the overall yield and oxidative behavior of ribose-containing nucleotides are extremely similar to those found in duplexes entirely composed of DNA, reflecting the significant pairwise stacking in RNA-containing duplexes.

## ACKNOWLEDGMENT

D.T.O. thanks the Parson's Foundation for a predoctoral fellowship.

## REFERENCES

1. Núñez, M. E., Hall, D. B., and Barton, J. K. (1999) *Chem. Biol. 6*, 85−97.
2. Giese, B. (2000) *Acc. Chem. Res. 33*, 631−636.
3. Giese, B., Meggers, E., Wessely, S., et al. (2000) *Chimia 54*, 547−551.
4. Núñez, M. E., and Barton, J. K. (2000) *Curr. Opin. Chem. Biol. 4*, 199−206.
5. Schuster, G. B. (2000) *Acc. Chem. Res. 33*, 253−260.
6. Lewis, F. D., Liu, X. Y., Liu, J. Q., Hayes, R. T., and Wasielewski, M. R. (2000) *J. Am. Chem. Soc. 122*, 12037−12038.
7. Lewis, F. D., Liu, X. Y., Liu, J. Q., Miller, S. E., Hayes, R. T., and Wasielewski, M. R. (2000) *Nature 406*, 51−53.
8. Hall, D. B., Holmlin, R. E., and Barton, J. K. (1996) *Nature 382*, 731−735.
9. Porath, D., Bezryadin, A., de Vries, S., and Dekker, C. (2000) *Nature 403*, 635−638.
10. Fink, H. W., and Schonenberger, C. (1999) *Nature 398*, 407−410.
11. Wan, C., Fiebeg, T., Kelley, S. O., Treadway, C. R., Barton, J. K., and Zewail, A. H. (1999) *Proc. Natl. Acad. Sci. U.S.A. 96*, 6014−6019.
12. Holmlin, R. E., Dandliker, P. J., and Barton, J. K. (1997) *Angew. Chem., Int. Ed. Engl. 36*, 2715−2730.
13. Ames, B. N., Shigenaga, M. K., and Hagen, T. M. (1993) *Proc. Natl. Acad. Sci. U.S.A. 90*, 7915−7922.
14. Piette, J. (1991) *J. Photochem. Photobiol. B 11*, 241−260.
15. Simon, M. I., and Vunakis, H. V. (1962) *J. Mol. Biol. 4*, 488−499.
16. Storhoff, J. J., and Mirkin, C. A. (1999) *Chem. Rev. 99*, 1849−1862.
17. Li, X., Yang, X., Qi, J., and Seeman, N. C. (1996) *J. Am. Chem. Soc. 118*, 6131−6140.
18. Mao, C., Sun, W., Shen, Z., and Seeman, N. C. (1999) *Nature 397*, 144−146.
19. Winfree, E., Liu, F., Wenzler, L. A., and Seeman, N. C. (1998) *Nature 394*, 539−544.
20. Yang, X., Wenzler, L. A., Qi, L., Li, X., and Seeman, N. C. (1998) *J. Am. Chem. Soc. 120*, 9779−9786.
21. Sugiyama, H., and Saito, I. (1996) *J. Am. Chem. Soc. 118*, 7063−7068.
22. Burrows, C., and Muller, J. G. (1998) *Chem. Rev. 98*, 1109−1152.
23. Núñez, M. E., Rajski, S. R., and Barton, J. K. (2000) *Methods Enzymol. 319*, 165−188.
24. Hall, D. B., Kelley, S. O., and Barton, J. K. (1998) *Biochemistry 37*, 15933−15940.
25. Ly, D., Kan, Y., Armitage, B., and Schuster, G. B. (1996) *J. Am. Chem. Soc. 118*, 8747−8748.
26. Breslin, D. T., and Schuster, G. B. (1996) *J. Am. Chem. Soc. 118*, 2311−2319.
27. Ito, K. (1993) *J. Biol. Chem. 268*, 13221−13228.
28. Other DNA-binding molecules can induce the signature 5′-GG-3′ localized reaction at close range (*29*).
29. Hickerson, R. P., Prat, F., Muller, J. G., Foote, C. S., and Burrows, C. J. (1999) *J. Am. Chem. Soc. 121*, 9423−9428.
30. Hall, D. B., and Barton, J. K. (1997) *J. Am. Chem. Soc. 119*, 5045−5046.
31. Kelley, S. O., Boon, E. M., Barton, J. K., Jackson, N. M., and Hill, M. G. (1999) *Nucleic Acids Res. 27*, 4830−4837.
32. Boon, E. M., Ceres, D. M., Drummond, T. G., Hill, M. G., and Barton, J. K. (2000) *Nat. Biotechnol. 18*, 1096−1100.
33. Rajski, S. R., and Barton, J. K. (1999) *J. Am. Chem. Soc. 121*, 5615−5616.
34. Rajski, S. R., and Barton, J. K. (2000) *J. Biomol. Struct. Dyn. 11*, 285−295.
35. Beratan, D. N., Priyadarshy, S., and Risser, S. M. (1997) *Chem. Biol. 4*, 3−8.
36. Bixon, M., and Jortner, J. (2000) *J. Phys. Chem. B 104*, 3906−3913.
37. Bixon, M., Giese, B., Wessely, S., Langenbacher, T., Michel-Beyerle, M. E., and Jortner, J. (1999) *Proc. Natl. Acad. Sci. U.S.A. 96*, 11713−11716.
38. Berlin, Y. A., Burin, A. L., and Ratner, M. A. (2000) *J. Phys. Chem. A 104*, 443−445.
39. Felts, A. K., Pollard, W. T., and Friesner, R. A. (1995) *J. Phys. Chem. 99*, 2929−2940.
40. Henderson, P. T., Jones, D., Hampikian, G., Kan, Y., and Schuster, G. B. (1999) *Proc. Natl. Acad. Sci. U.S.A. 96*, 8353−8358.
41. Williams, T. T., Odom, D. T., and Barton, J. K. (2000) *J. Am. Chem. Soc. 122*, 9048−9049.
42. Kelley, S. O., and Barton, J. K. (1999) *Science 283*, 375−380.
43. Kelley, S. O., and Barton, J. K. (1998) *Chem. Biol. 5*, 413−418.
44. Kan, Y., and Schuster, G. B.(1999) *J. Am. Chem. Soc. 121*, 10857−10864.
45. Kan, Y., and Schuster, G. B. (1999) *J. Am. Chem. Soc. 121*, 11607−11614.
46. Núñez, M. E., Noyes, K. T., Gianolio, D. A., McLaughlin, L. W., and Barton, J. K. (2000) *Biochemistry 39*, 6190−6199.
47. Roberts, R. W., and Crothers, D. M. (1992) *Science 258*, 1463−1470.
48. Salazar, M., Fedoroff, O. Y., Miller, J. M., Ribeiro, N. S., and Reid, B. R. (1993) *Biochemistry 32*, 4207−4215.
49. Gyi, J. I., Conn, G., Lane, A. N., and Brown, T. (1996) *Biochemistry 35*, 12538−12548.
50. Gyi, J. I., Lane, A. N., Conn, G., and Brown, T. (1998) *Nucleic Acids Res. 26*, 3104−3110.
51. Lesnick, E. A., and Freier, S. M. (1995) *Biochemistry 34*, 10807−10815.
52. Wang, A., Fujii, S., van Boom, J. H., van der Marel, G. A., Boeckel, S. A. A., and Rich, A. (1992) *Nature 299*, 601−604.
53. Sartor, V., Henderson, P. T., and Schuster, G. B. (1999) *J. Am. Chem. Soc. 121*, 11027−11033.
54. Holmlin, R. E., Dandliker, P. J., and Barton, J. K. (1999) *Bioconjugate Chem. 10*, 1122−1130.

55. Olmstead, J., and Kearns, D. R. (1977) *Biochemistry 16*, 3647−3654.
56. LepPecq, J. B., and Paoletti, C. (1967) *J. Mol. Biol. 27*, 87−106.
57. Lim, A. C., and Barton, J. K. (1993) *Biochemistry 32*, 11029.
58. Chow, C. S., and Barton, J. K. (1990) *J. Am. Chem. Soc. 112*, 2839.
59. Sitlani, A., and Barton, J. K. (1994) *Biochemistry 33*, 12100.
60. Egli, M., Usman, N., Zhang, S., and Rich, A. (1992) *Proc. Natl. Acad. Sci. U.S.A. 89*, 534−548.
61. Egli, M., Usman, N., and Rich, A. (1993) *Biochemistry 32*, 3221−3227.
62. Prat, F., Houk, K. N., and Foote, C. S. (1998) *J. Am. Chem. Soc. 120*, 845−846.
63. Sugiyama, H., and Saito, I. (1996) *J. Am. Chem. Soc. 118*, 7063−7068.

BI0102961